Decoupling of critical temperature and superconducting gaps in irradiated films of a Fe-based superconductor

Dario Daghero[1]**, Mauro Tortello**[1]**, Giovanni A Ummarino**[1,2]**,**
Erik Piatti[1]**, Gianluca Ghigo**[1,3]**, Takafumi Hatano**[4]**, Takahiko Kawaguchi**[5]**,**
Hiroshi Ikuta[4] **and Renato S Gonnelli**[1]

[1] Dipartimento di Scienza Applicata e Tecnologia, Politecnico di Torino, Corso Duca degli Abruzzi 24, I-10129, Torino, Italy
[2] National Research Nuclear University MEPhI, Moscow Engineering Physics Institute, Moscow, Russia
[3] Istituto Nazionale di Fisica Nucleare, Sezione di Torino, I-10125, Torino, Italy
[4] Department of Materials Physics, Nagoya University, Nagoya 464-8603, Japan
[5] Department of Electronics and Materials Science, Shizuoka University, Hamamatsu 432-8561, Japan

E-mail: dario.daghero@polito.it

CrossMark

Abstract
We report on direct measurements of the energy gaps (carried out by means of point-contact Andreev reflection spectroscopy, PCARS) and of the critical temperature in thin, optimally doped, epitaxial films of $BaFe_2(As_{1-x}P_x)_2$ irradiated with 250 MeV Au ions. The low-temperature PCARS spectra (taken with the current flowing along the c axis) can be fitted by a modified Blonder–Tinkham–Klapwijk model with two nodeless gaps; this is not in contrast with the possible presence of node lines suggested by various experiments in literature. Up to a fluence $\Phi = 7.3 \times 10^{11}\,cm^{-2}$, we observe a monotonic suppression of the critical temperature and of the gap amplitudes Δ_1 and Δ_2. Interestingly, while T_c decreases by about 3%, the gaps decrease much more (by about 37% and 25% respectively), suggesting a decoupling between high-temperature and low-temperature superconducting properties. An explanation for this finding is proposed within an effective two-band Eliashberg model, in which such decoupling is inherently associated to defects created by irradiation.

Keywords: superconducting energy gaps, effects of irradiation, superconducting thin films, Fe-based superconductors, Point-contact Andreev-reflection spectroscopy, multi-band superconductivity, Eliashberg equations

(Some figures may appear in colour only in the online journal)

1. Introduction

Irradiation of iron-based superconductors with different kinds of particles (electrons, protons, neutrons, ions, α particles) has been used in the past few years to tune some physical parameters of interest for applications (critical current, irreversibility field) but also to gain some insight into the nature of the electronic coupling that gives rise to the formation of Cooper pairs in these compounds [1–4]. The effect of disorder on the critical temperature is indeed predicted to depend on the symmetry of the superconducting gap (i.e. $s\pm$ or $s++$), on the presence or absence of nodes in the gap, and on the ratio between *interband* and *intraband* scattering rates [5]. Recently, a disappearance and reappearance of the small gap in $Ba(Fe,Co)_2As_2$ films irradiated with protons has been observed [6], which would point towards a transition from $s\pm$ to $s++$ induced by disorder as predicted when the electron–electron coupling constant averaged over the Fermi surface is positive [7]. Similarly, a change in the sign of the small gap has been deduced from penetration-depth

measurements in $(Ba,K)Fe_2As_2$ crystals irradiated with 250 MeV Au ions [4].

In a recent paper [8], we have studied the effects of 250 MeV Au-ion irradiation on the morphological, structural and superconducting properties of isovalent-doped $BaFe_2(As_{1-x}P_x)_2$ epitaxial thin films. As shown in the case of $Fe(Se,Te)$ [9] and $Ba(Fe,Co)_2As_2$ [10] crystals, irradiation with heavy ions creates correlated defects along the ions' trajectory, and a cloud of point-like defects due to secondary electrons generated in ion-atom collisions. Correlated or columnar defects play a fundamental role in pinning of vortexes and thus enhance both the critical current and the irreversibility field [10], while point-like defects are the main responsible for the increase in resistivity [9].

In the case of thin films, as we have shown in [8], the situation is considerably complicated by the role played by the substrate. As a matter of fact, T_c decreases very little upon irradiation, while the residual resistivity ρ_0 increases considerably. The dependence of the normalized T_c on $\Delta\rho_0$ is thus very weak and would apparently be compatible with a nodeless $s\pm$ gap symmetry. However, studies of the same material (in the form of crystals) irradiated with electrons [2] indicate a much larger decrease in the critical temperature for a similar enhancement of residual resistivity [8], as expected for a nodal $s\pm$ symmetry. Indeed, the presence of nodes in the gap of $BaFe_2(As_{1-x}P_x)_2$ is suggested by various experiments that detect zero-energy quasiparticle states [11–14] even though the exact shape of the node lines and even their location on the Fermi surface is still debated [15–18].

In this particular situation, the normal-state transport properties and the superconducting critical temperature appear to be somewhat decoupled. This behaviour could be ascribed to the defected substrate that might amplify the effect of irradiation by creating additional scattering centres. This also means that any comparison of the results obtained in thin films with theories developed to describe single crystals must be always taken with caution. It is thus particularly interesting to see whether the amplitudes of the energy gaps, which are the fundamental quantities characterizing the low-temperature superconducting state, follow the trend of the critical temperature (and thus are weakly or negligibly suppressed by irradiation), or, rather, are sensitive to the same defects that are responsible for the increase of resistivity (and thus are strongly decreasing as a function of Au-ion fluence).

In this paper we address this question by measuring the gap amplitude in epitaxial thin films of P-doped Ba-122 using point-contact Andreev-reflection spectroscopy. The spectra show rather clear structures associated to (at least) two energy scales corresponding to superconducting gaps, and the amplitudes of these gaps decrease by more than 30% upon Au-ion irradiation (up to a fluence $\Phi = 7.3 \times 10^{11}\,\mathrm{cm}^{-2}$) while the critical temperature decreases by at most 3%. This huge difference in the rate of suppression has the obvious consequence that the gap ratios strongly decrease. Although this decrease suggests a suppression of the superconducting coupling strength, it is not easy to understand how this can be reconciled with the persistence of T_c's as high as 30 K in the irradiated films. Again, we propose an explanation of this puzzle based on the presence of defects created by irradiation

within the film *and* induced by the substrate, which make the density of states available for pairing depend on temperature. This is an interesting and rarely observed case of decoupling between the critical temperature and the superconducting gap amplitudes.

2. Experimental details

2.1. Thin films

We used three different $BaFe_2(As_{1-x}P_x)_2$ thin films, in the following labelled as N.360, N.316 and N.686, with a thickness of 50 ± 5 nm. All of them were grown at 850 °C on top of MgO single crystal substrates by molecular beam epitaxy using a background pressure of 10^{-7} Pa. As described in [19, 20], all the elements were supplied from Knudsen cells. Pure metallic sources were used for Ba, Fe, and As, while GaP was used for phosphorous (Ga being removed by two trapping caps placed on the crucible, so as to obtain an almost pure P flux). The P content x of the films was controlled by tuning the P vapour pressure while keeping the As vapour pressure constant, and the actual stoichiometry of the final films was checked by electron probe micro-analysis. The actual P content was $x = 0.19$ for films N.316 and N.686, and slightly larger ($x = 0.20$) for film N.360. Unlike in bulk and crystals, these doping levels correspond to the top of the superconducting dome in the case of these films [8, 19]. As a matter of fact, the critical temperature of the pristine films is indeed very high, always above 30 K. The shift of the phase diagram along the horizontal (P content) axis if compared to that of single crystals is due to the presence of an in-plane tensile strain that, in turns, originates from the lattice mismatch between the $BaFe_2(As,P)_2$ film and the underlying MgO substrate [19]. This mismatch is effective because: (i) the films grow with the c axis of $BaFe_2(As,P)_2$ perpendicular to the film surface, as proved by x-ray diffraction spectra that only display 00ℓ reflections of $BaFe_2(As,P)_2$ besides the peaks from the substrate; (ii) the films also have an in-plane orientation, with the a axis of $BaFe_2(As,P)_2$ parallel to the a axis of MgO, as shown by ϕ-scans of the 103 peak [19]. The mismatch, though not preventing the epitaxial growth, is rather large. In pure $BaFe_2As_2$ it is 6.30% but increases with the P content, becoming as large as 9.58% in pure $BaFe_2P_2$ [19, 21]. As a consequence of the strain, the c-axis lattice parameter of the films is shorter than that of the single crystals. In particular, its value (obtained through a refinement of the x-ray diffraction (XRD) spectra) is $c = 12.770 \pm 0.005$ Å for film N.316, $c = 12.795 \pm 0.009$ Å for film N.686, and $c = 12.766 \pm 0.002$ Å for film N.360. These values must be compared with the value in crystals, i.e. $c_{\mathrm{bulk}} = 12.88$ Å [22].

2.2. Irradiation

Each film was initially characterized as a whole by means of four-probe transport measurements, using collinear and van der Pauw [23, 24] contact configurations in order to test the homogeneity on the millimeter scale. Then, it was divided into
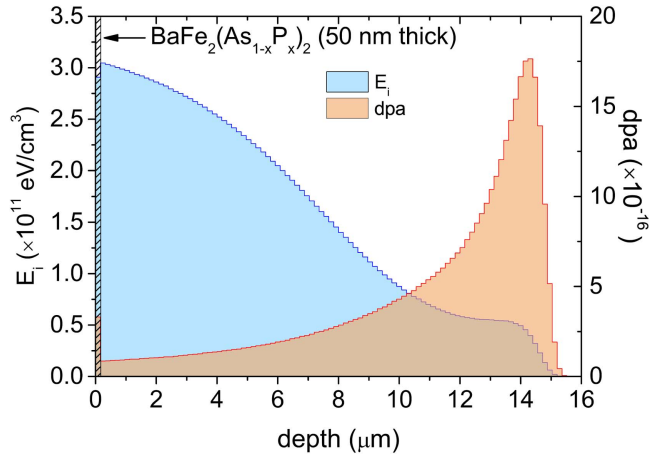
Figure 1. Expected damage calculated by means of the code SRIM-2013, in terms of energy released through ionization, E_i (related to the electron scattering), and of displacements per atom (dpa) (due to the Coulombian scattering against target nuclei) in a 50 nm-thick P-doped Ba-122 film and in its MgO substrate, produced by a single 250 MeV Au ion over an area of 1 cm^2. The E_i and dpa values for each sample can be calculated by multiplying these values by fluence, expressed in cm^{-2}. The width of the first depth class, corresponding to the superconducting film (50 nm), is not to scale.

four parts, three of which were irradiated with 250 MeV Au-ions at the TandemXTU accelerator of INFN-LNL (Istituto Nazionale di Fisica Nucleare-Laboratori Nazionali di Legnaro) [25] with fluences $\Phi_1 = 2.4 \times 10^{11}$ cm^{-2}, $\Phi_2 = 4.8 \times 10^{11}$ cm^{-2} and $\Phi_3 = 7.3 \times 10^{11}$ cm^{-2}, corresponding to dose equivalent fields of 5, 10 and 15 T, respectively. To minimize the heating of the samples under irradiation, the ion flux was always kept below 2.0×10^8 cm^{-2} s^{-1}. The direction of the ion beam was parallel to the c axis of the films. In iron-based superconducting materials, 250 MeV Au-ion irradiations were proved to produce both correlated and point defects [9] due to Coulombian scattering of the incoming ions against the electrons and the nuclei of the target. In our samples (film and substrate) the expected damage was estimated by means of the Monte-Carlo code SRIM-2013 [26, 27], in terms of energy released by ionization, E_i, and displacements per atom (dpa) due to the elastic Coulombian scattering against target nuclei. This calculation was carried out using the modified Kinchin–Pease approach [28, 29]. Along the nanometric thickness of the film, damage results to be uniform, with $E_i = 2.9 \times 10^{11} \times \Phi$ eV cm^{-3} and dpa $= 3.3 \times 10^{-16} \times \Phi$, respectively, with the fluence Φ expressed in cm^{-2}. Into the MgO substrate, E_i and dpa show dependence on depth (see figure 1), up to implantation at a depth of 14.5 ± 0.5 μm. The large energy lost in the substrate and the elevated value of dpa in the implantation region are proved to modify the substrate lattice; indeed, the width of the MgO peak in the XRD spectra increases upon irradiation (see figure 2 of [8]). This, in turn, is expected to affect the superconducting film properties through a modification of the strain. As a matter of fact, atomic force microscope measurements show that the very smooth surface of the pristine films (with clear interconnected terraced structures) is progressively damaged by irradiation [8].

Noticeably, the appearance of localized defects in the form of small cracks (already at the lowest irradiation fluence) can be associated to the partial relaxation of the strain induced by the damage of the substrate (see [8] and references therein). This should be taken into account in comparing the effect of ion irradiation in films and single crystals.

2.3. Critical temperature

In [8] we discussed the behaviour of the critical temperature of films N.316 and N.360, determined from transport measurements, as a function of the fluence. The film N.686 follows the same trend. Figure 2(a) shows the critical temperature (here defined as the temperature at which the resistance drops to 90% of its normal-state value, i.e. T_c^{90}) as a function of the dpa (bottom scale) and of the ionization energy E_i (top scale). E_i and dpa express better than the fluence the damage due to electronic and nuclear scattering; moreover their use allows a comparison of data coming from different irradiation experiments.

The T_c of the pristine films N.316 and N.686 (that have the same P content $x = 0.19$) is practically identical, while that of the film N.360 is slightly smaller because of the different doping content. Upon irradiation, the variation in T_c is the same for all the three films (which is a confirmation of the reproducibility of the results) and is equal to about 1 K on going from the pristine to the most irradiated film. Of course, because of the slight difference between the critical temperatures of the pristine films, the relative T_c variations slightly differ. Figure 2(b) shows the values of T_c normalized, for each film, to that of the unirradiated (pristine) part. It is clear that in the worst case the critical temperature decreases by 3%, which is a very small amount indeed. As for the width of the transition, defined as $T_c^{90} - T_c^{10}$, we have already shown for N.316 and N.360 [8] that it increases very slightly upon irradiation, going from about 0.5 K in the pristine films to about 0.7 K in the most irradiated ones. The case of film N.686 is slightly different: its transition is already wider before irradiation (of the order of 1.5 K) and approximately doubles at the highest irradiation dose. As a result, on going from the pristine to the most irradiated film, the values of T_c^{10} decrease by 3% in film N.316, by 2.5% in film N.360 [8] and by 8% in film N.686.

2.4. Determination of the energy gaps

The energy gaps in the pristine and irradiated films were measured by using point-contact spectroscopy in the regime of large barrier transparency, when the conduction through the point contacts is dominated by Andreev reflection, hence the name of 'point-contact Andreev reflection spectroscopy' (PCARS). The technique consists in recording the differential conductance as a function of the bias voltage (i.e. the dI/dV versus V curve) of a small (point-like) contact between a normal metal and the superconductor under study (in this case the film). A fit of the spectrum obtained in this way by means of suitable models provides information on the number,
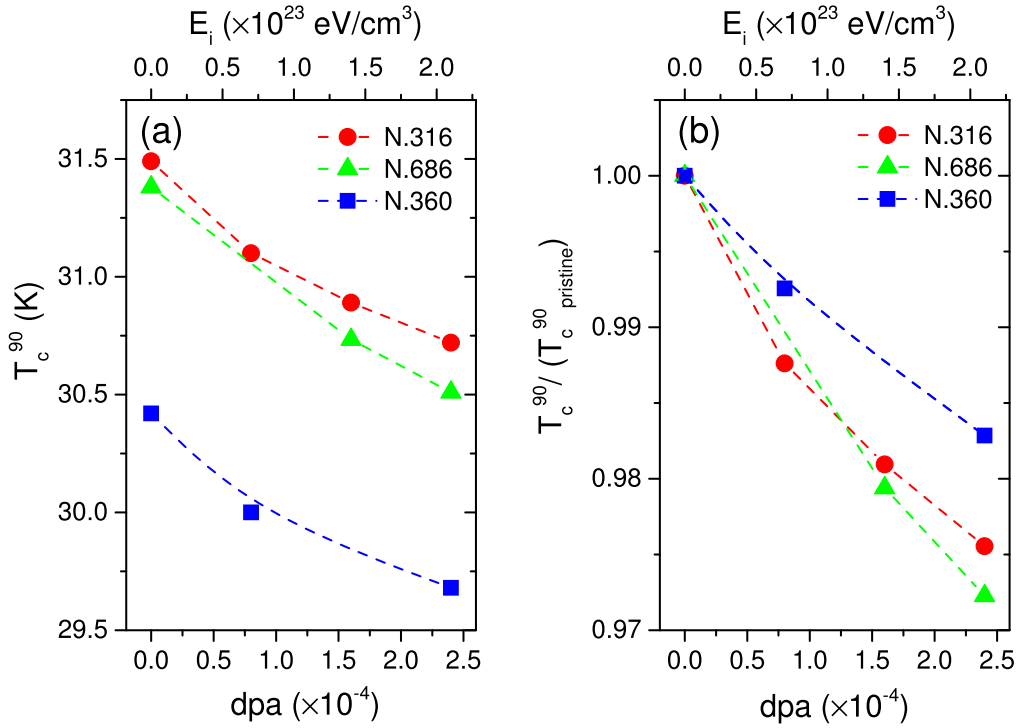
Figure 2. Critical temperatures, T_c^{90}, as a function of the energy released by ionization, E_i (top horizontal axis), and of the displacements per atom (dpa, bottom horizontal axis) induced by elastic scattering against target nuclei for the films N.316, N.686 and N.360. (a) Absolute values; (b) values normalized to T_c^{90} of the pristine film. The values of dpa and E_i correspond to the fluences $\phi_1 = 2.4 \times 10^{11}\,\mathrm{cm}^{-2}$, $\phi_2 = 4.8 \times 10^{11}\,\mathrm{cm}^{-2}$ and $\phi_3 = 7.3 \times 10^{11}\,\mathrm{cm}^{-2}$.

amplitude and (to some extent) structure of the gap(s) in the reciprocal space.

To make the point contacts, we used the 'soft' technique, in which a thin Au wire ($\varnothing = 18\,\mu$m) is kept in contact with the film surface by means of a small drop ($\varnothing \leqslant 50\,\mu$m) of Ag conducting paste. This technique works particularly well in the case of thin films, as shown for Co-doped Ba-122 [30] and Fe(Se,Te) [31], while the standard needle-anvil technique (in which the contact is made by gently pressing a metallic tip or wire against the sample surface) generally leads to unstable contacts and risks piercing the film if the applied pressure is too large. The fact that the surface of the films may be covered by a thin oxidation layer is not necessarily detrimental to the soft PCARS measurements, as shown in [30, 31], since the actual electrical contact between the grains of the Ag paste and the film can occur only here and there, through pinholes in the oxide layer. This creates a parallel of several contacts that can be, individually, nanometric in size but are spread over an area of about 2500 μm^2.

There are various consequences of this fact: (i) the spectra contain information about a finite area of the sample surface, i.e. they are in some sense an average of the signals coming from different nanometric contacts; (ii) the apparent size of the contact as a whole is only loosely related to its resistance. Not necessarily bigger Ag drops correspond to smaller resistance; (iii) the resistance itself is not directly associated to the size of the *individual* contacts, as it would be if only one single contact were established between the film and the counterelectrode. In that case, it would be possible to

determine whether the conduction through the contact is ballistic (ideal case) or not, by estimating the contact size using either the Sharvin [32] or, better, the Wexler [33] equation that, for a heterocontact between two materials labelled 1 and 2 reads [34]

$$R \simeq R_S + R_M = \frac{2h}{e^2 a^2 k_{F,min}^2 \tau} + \frac{\rho_1 + \rho_2}{4a}. \qquad (1)$$

Here a is the radius of the contact (modelled as a circular aperture in an otherwise completely opaque interface between the two materials), ρ_i is the resistivity of the ith bank, $k_{F,min}$ is the smaller Fermi wavevector between k_{F1} and k_{F2}, and τ is a function of the Fermi velocities v_{F1} and v_{F2}, i.e. $\tau = 4v_{F1}v_{F2}/(v_{F1} + v_{F2})^2$. The first term, called Sharvin resistance, is temperature-independent and would correspond to a perfectly ballistic contact ($a \ll \ell$, where ℓ is the electronic mean free path) which is the ideal condition for energy-resolved spectroscopy in both the normal and the superconducting state [35]. The second term is the Maxwell resistance and is dominant when $a \gg \ell$; in these conditions, heating occurs in the contact region and no spectroscopic information can be extracted. Note that R_M depends on temperature through ρ_1 and ρ_2. If $\rho_2 = 0$ (i.e. the material 2 is superconducting) this term contains only the resistivity of the normal metal (usually Au or Ag, as in our case). An additional condition on a is that $a < \xi$ (ξ being the coherence length) [36, 37] which prevents the disruption of superconductivity by the current flowing through the contact.

In the case of a Ag-paste contact on a film, evaluating the contact size from its resistance is a procedure that makes no sense and would only provide an upper limit for the size of the individual contacts. Thus, the determination of the spectroscopic regime can only be made *a posteriori* by looking at the shape of the spectra. As will be shown later, most of our contacts lie in an intermediate regime [34] in which spectroscopy is still possible at low temperature (where the mean free path is maximum and $\rho_2 = 0$) and low voltage bias (where the current is less than critical). In many cases, the Andreev signal is smaller than expected, either because of elastic scattering in the contact (diffusive regime [34, 35]) or because, in irradiated samples, a fraction of the parallel nanocontacts actually occur on defected (normal) regions of the film. On increasing voltage and/or temperature, anomalous effects make the contacts depart from ideality: typical dips [38] signal the current-induced breakdown of superconductivity, while a downward shift of the conductance curves (accompanied by their horizontal stretching) occurs when ρ_2 departs from zero and a spreading resistance [39] appears. In general, the latter can come from both R_M and the portion of film between the point contact and the second voltage electrode (see the inset to figure 3(b)), whose resistance can be comparable to that of the contact itself because of the small thickness [31, 40].

As an example, figure 3(a) shows a series of PCARS spectra taken at different temperatures, in the most irradiated part of the film N.360. The normal-state resistance of the contact (determined at 30 meV) is $R_N \simeq 25\,\Omega$. The curves show clear Andreev-reflection features in the form of a conductance enhancement around zero bias. The low-temperature spectra show symmetric (shallow) maxima at about ± 2 mV, which suggest that the contact is in the spectroscopic regime at these bias values. At higher voltage, there is no sign of anomalies associated to the breakdown of superconductivity [38] so that one can rather safely assume that the contact *is* in the spectroscopic regime. The small downward curvature of the tails may suggest a small contribution from the Maxwell term $\rho_1/4a$. However, on increasing the temperature up to 27 K, the high-voltage tails of the spectra are superimposed, indicating the absence of a temperature dependence in the normal-state contact resistance and thus suggesting a Sharvin regime. Above this temperature, the curves start to shift downward, and are progressively stretched along the horizontal scale [39] because of the temperature-dependent spreading resistance. The connection between the resistive transition and the shift of the conductance curves is clear if one plots the high-voltage resistance extracted from the spectra as a function of temperature and compares it to the $\rho(T)$ curve, as in figure 3(b). The inset to the graph depicts a scheme of the pseudo-four probe arrangement used for PCARS; the spreading resistance in this case only comes from the portion of film between the point contact and the first voltage electrode. Note that the dots depart from the low-temperature values (i.e. the conductance curves start to shift) a little before the onset of non-zero resistivity. This is an effect of the current: while in PCARS measurements the current flowing through the sample at 30 mV is 1.2 mA, the current
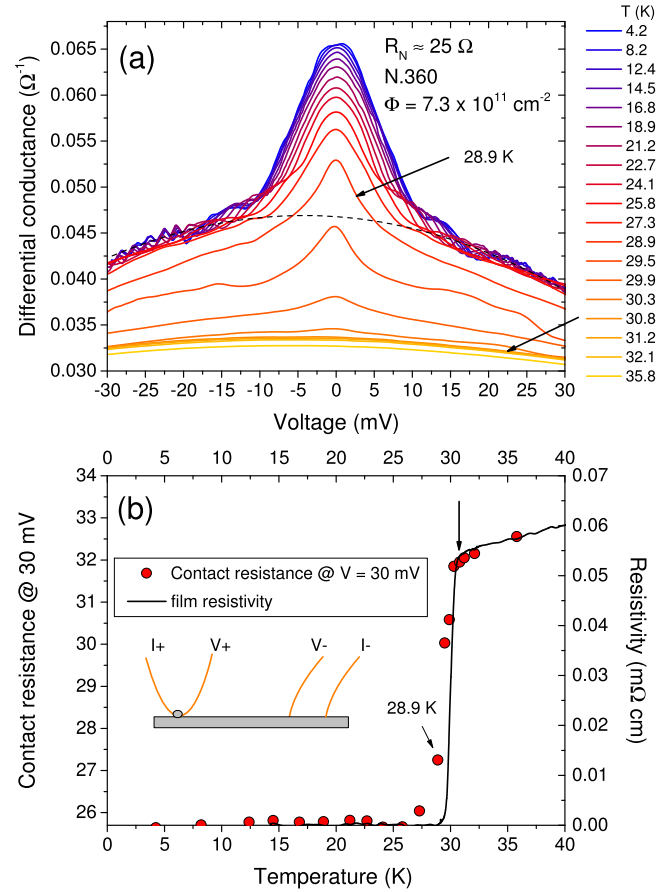

Figure 3. (a) Temperature dependence of the conductance curve dI/dV of a point contact with normal-state resistance (at low temperature) $R_N \simeq 25\,\Omega$, made on the most irradiated part of the film N.360. The dashed line represents the second-order polynomial that fits the high-energy tails (eV > 15 meV) of the lowest-temperature conductance curve. (b) Comparison between the film resistivity (line, right-hand vertical axis) and the contact resistance calculated as the inverse of the conductance at 30 mV (dots, left-hand vertical axis).

used for the resistivity measurement was much smaller (10 μA).

The shift and deformation of the conductance curves makes a clear determination of the local critical temperature of the contact (the so-called Andreev critical temperature, T_c^A) rather difficult. In the case of crystals or bulk samples (where the spreading resistance is negligible) T_c^A is defined as the temperature at which the Andreev features disappear and the conductance curves start to be superimposed. In general, it falls within the width of the superconducting transition measured by transport. Here, the conductance curves become superimposed at 30.8 K, when the spreading resistance ceases to be strongly temperature dependent—i.e. at the onset of the superconducting transition (see arrows in figure 3). Hence, the temperature where this happens correlates well with T_c^{90}, but does not necessarily coincide with the critical temperature of the contact alone, T_c^A, that could be slightly smaller. We can identify a lower boundary for T_c^A by looking at the conductance at zero bias; as long as this falls above the presumed low-temperature 'normal state' (obtained by fitting the

high-energy tails of the conductance curves not affected yet by the vertical shift: see the dashed line in figure 3(a)), the contact is certainly still superconducting and Andreev reflection occurs. In the case of figure 3, this holds true for the conductance curve recorded at 28.9 K, that approximately corresponds to T_c^{10}. This correspondence is always verified so that we can safely say that the T_c^A of a contact is lower-bounded by the T_c^{10} of the film; hence, at the highest fluence the critical temperature of the contacts can decrease *at most* by 8% in film N.686, by 3% in film N.316, by 2.5% in film N.360.

The shift and deformation of the conductance curves due to the spreading resistance also prevents the use of the normal-state conductance measured at T_c for the normalization of the low-temperature spectra, which is necessary in order to compare them to the models for Andreev reflection at the N/S interface. Each spectrum should be thus normalized by the normal-state conductance curve measured at the same temperature. This is experimentally inaccessible at low temperature because of the high critical field of the films, and therefore a guess has to be made for the low-temperature normal state conductance curve, as already mentioned in [30]. One possibility consists in taking the normal-state conductance curve measured just above T_c (i.e. at 30.8 K in the case of figure 3(a)), compress its horizontal scale, and translate it upwards in order to get rid of the effects of the spreading resistance. Another possibility (that in the best cases practically coincides with the previous one, but cannot be used if the conductance curves display dips or high-bias anomalies) is to define the 'normal state' by finding a second-order polynomial that fits the high-energy tails of the curves [30, 31] (see for example the dashed line in figure 3(a)). In general, to account for the degree of arbitrariness in this guess, we actually normalized each conductance curve in different ways, and fitted the resulting spectra so as to obtain a range of possible gap values compatible with that curve. Some examples of normalized conductance curves $((dI/dV)_{NS}/(dI/dV)_{NN}$ versus V) measured at low temperature in films at different levels of irradiation are reported in figure 4 as blue dots (the fluence is indicated in the labels).

To obtain the gap amplitudes, the normalized conductance curves were fitted with the Blonder–Tinkham–Klapwijk (BTK) model generalized by Kashiwaya and Tanaka [41, 42] (later on called '2D BTK model'). This model contains three parameters for each gap: the gap amplitude Δ, the barrier parameter Z (that accounts for the transparency of the barrier at the N/S interface) and the broadening parameter Γ [43]. The first problem is how many gaps should be used for the fit. Even if a single gap amplitude of about 5 meV has been recently measured in $BaFe_2(As_{1-x}P_x)_2$ crystals with $T_c \simeq 30$ K by optical transient reflectivity [44] and nanocalorimetry [14], a single-gap model is unable to fit the PCARS conductance curves in the pristine and in the irradiated films. In most cases, the curves show symmetric conductance maxima *and* additional shoulders at higher energy, a typical sign of (at least) two gaps. Even when the shoulders are less visible, however, the single-gap fit is unable to capture the shape of the spectra, as shown by the dashed lines in figures 4(a) and (e). The minimum number of gaps that

allows a good fit of the spectra is thus 2; in this case the model contains seven parameters, three for each gap and the relative weight of the two gaps in determining the signal. The number of parameters makes the fit be non-univocal, meaning that there is normally a range of fitting parameters for a single experimental curve, which results in an uncertainty on the gap values [30, 31] anyway smaller than that due to the choice of the normalization. The various parameters are not completely independent in the sense that there is some degree of interplay between their effects; however, there is also a number of constraints such as: (i) the amplitude of the spectrum; (ii) the energy position of the conductance peaks; (iii) the energy position of the shoulders; (iv) the height of the shoulders; (v) the depth of the zero-bias dip. In order not to underestimate the effect of the large number of parameters, we first find a best fit that is obtained by minimizing the sum of squared residuals, and then we try to maximize (minimize) each of the gaps while changing all the other parameters as well—while maintaining the fit within a given level of confidence. This procedure, already used and explained elsewhere (see, e.g. [30, 34, 45, 46]) gives us a range of gap values compatible with the given curve. We then take the midpoint of this range as the 'true' value of the gap and half of the amplitude of the range itself as the uncertainty. When different choices of the 'normal state' give rise to different values of the gaps, the range also includes the uncertainty arising from the normalization.

The solid lines in figure 4 represent the best fit of the spectra obtained with the two-band 2D BTK model. The relevant values of the gaps Δ_1 and Δ_2 are indicated in the label of each panel (note that these values refer to *that* particular fit of the spectrum normalized in *that* particular way). In general, the amplitude of the Andreev signal is not very high and far from ideal. This is rather common in thin films, as was observed in the case of Co-doped Ba-122 [30] and Fe(Se, Te) [31]. To obtain a reasonable fit, rather large values of the broadening parameters Γ_1 and Γ_2 are necessary—although the condition $\Gamma_i < \Delta_i$, generally assumed to be essential for a meaningful fit, is always fulfilled.

Sometimes, the contacts are spectroscopic at low voltage but depart from ideality on increasing voltage, showing dips or a sudden downward deviation. This indicates that at these voltages the current density exceeds the critical value and superconductivity is disrupted. This is not detrimental to the determination of the gap amplitudes provided that such effect occurs sufficiently far from the Andreev features, i.e. at sufficiently high voltage. An example of this situation is reported in panel (d). The spectrum in (h) also presents a deviation from ideality, which is actually a very wide dip starting at 20 mV. In other cases, as in panels (e), (c) and (g), the experimental spectra present high-energy shoulders that are the hallmark of the strong electron–boson coupling typical of Fe-based compounds [31, 47, 48] but cannot be reproduced by the 2D BTK model, which is based on the weak-coupling theory of superconductivity. In particular, the energy position of these shoulders is determined by the amplitude of the gaps *and* by the characteristic energy of the mediating boson (here $\Omega_0 = 4.65 k_B T_c \simeq 12.5$ meV [49]) as explained in [48].
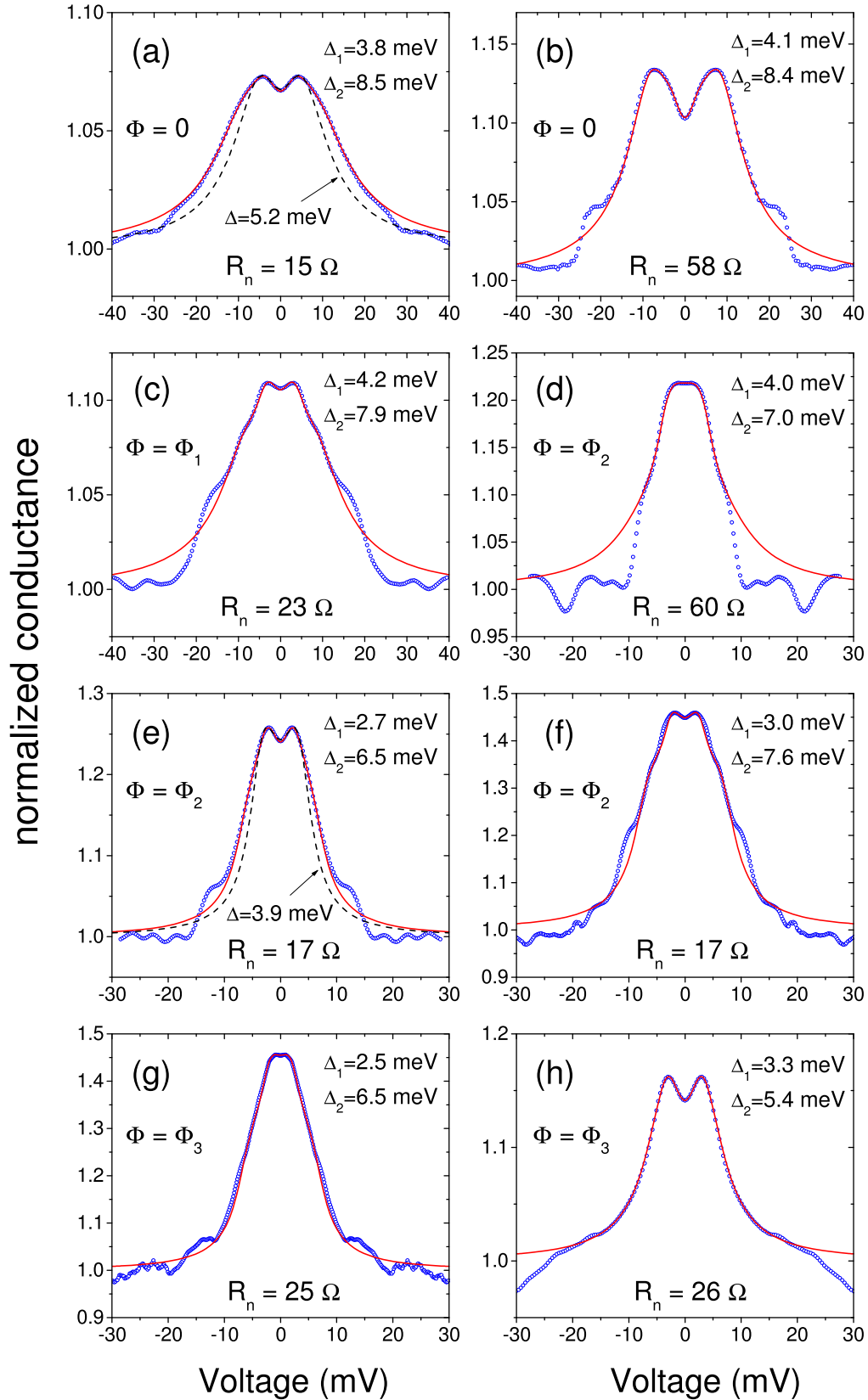
Figure 4. Examples of experimental PCARS spectra (blue dots) measured at low temperature (4.2 K) in different films and at different fluences (indicated in the labels): $\phi_1 = 2.4 \times 10^{11}$ cm^{-2}, $\phi_2 = 4.8 \times 10^{11}$ cm^{-2} and $\phi_3 = 7.3 \times 10^{11}$ cm^{-2}. Red solid lines: best fit of the experimental curves within the two-band, 2D BTK model. The amplitudes of the two gaps Δ_1 and Δ_2 are reported in the labels. In panels (a) and (e) a fit with a single-gap 2D BTK model is also reported (black dashed lines), with the relevant gap amplitude Δ.
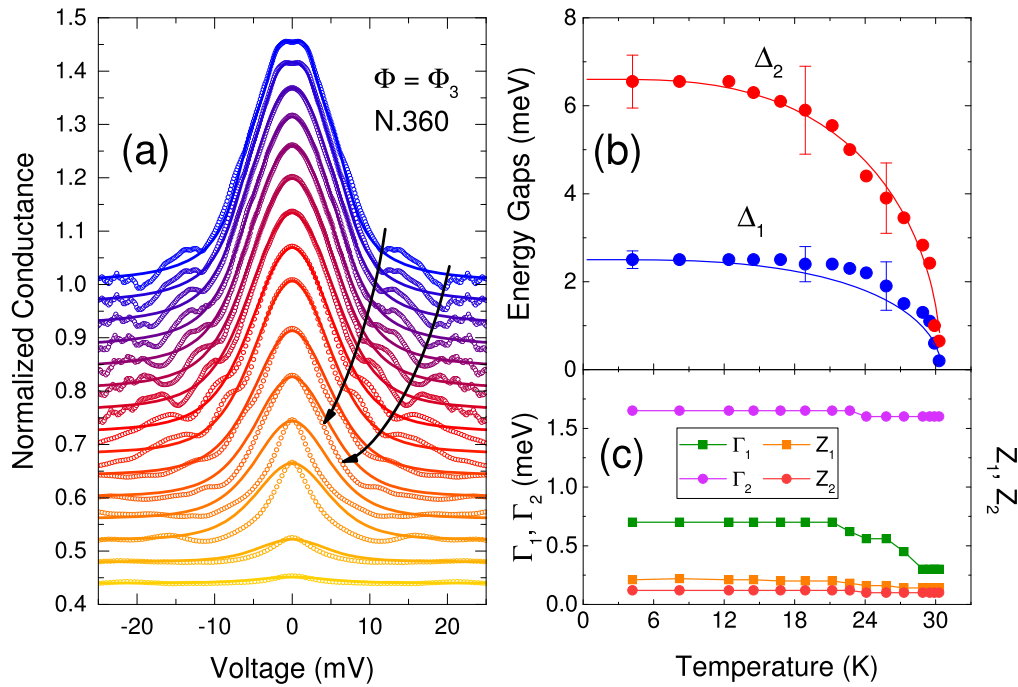
Figure 5. (a) Symbols: PCARS spectra of a point contact on the most irradiated part of the film N.360 ($\Phi = \Phi_3 = 7.3 \times 10^{11}$ cm^{-2} measured at different temperatures. These spectra were obtained by normalizing the curves in figure 3(a). The spectra are vertically offset for clarity. Lines: best-fit of the spectra within the two-band, 2D BTK model. (b) Temperature dependence of the gap amplitudes extracted from the fit. The uncertainty, here evaluated only by varying the fitting parameters without changing the normalization, is shown for three temperatures. Lines represent the BCS-like temperature dependences for comparison. (c) Temperature dependence of the other fitting parameters, i.e. Γ_1, Γ_2, Z_1 and Z_2.

We know from ARPES [16] that there are actually five different gaps in this compound, associated to the three holelike and the two electronlike Fermi surfaces (FS). As for the gaps on the holelike FS, in an ARPES study using synchrotron radiation [16] they were found to vary along the k_z axis from $k_z = 0$ to $k_z = \pi$ [16] ranging from 8 meV to about 6 meV on the β Fermi surface sheet, from 6 meV to about 5 meV on the γ sheet, and from about 8 meV to zero for the α Fermi surface sheet. The latter gap was therefore claimed to display a node line in the $k_z = \pi$ plane. In the same paper, the gaps on the electronlike FS sheets δ and η turned out to be homogeneous with values of about 8 meV and 6 meV, respectively. In a bulk-sensitive laser ARPES study, however, a finite gap of about 3–4 meV was found at $k_z = \pi$ and $k_z = 0$ for all the three holelike FS, in stark disagreement with the aforementioned findings, and indicating that the gaps are not only orbital-independent but also k_z-independent [15, 17]. In no case an in-plane anisotropy of the gaps on the holelike FSs was found. More recently, another ARPES study has confirmed the isotropy of the gaps on the holelike FSs (with a k_z-independent amplitude of about 6.5 ± 1.5 meV) and the absence of node lines, however claiming a strong anisotropy and possible node loops on the inner electronlike Fermi surface [18]. A very rough estimation of the gap (using the crossing point between the energy-dispersive curves below and above T_c) gives a value that ranges between 2 and 6 meV on the inner electronlike FS, and between 2 and 4 meV on the outer one.

These controversial results do not provide a sound term of comparison for our gap values. Considering that PCARS is only sensitive to the amplitude of the gaps, that it is unable to discriminate between gaps of equal amplitude that pertain to different Fermi surface sheets, and that its resolution is about $k_B T \simeq 0.3$ meV at low temperature, the values we obtain in the pristine films (about 8 meV and about 4 meV) seem anyway to be compatible with those observed in different ARPES studies.

A final remark about the 2D BTK model is that it is based on the assumption of spherical FS, which is clearly not true in Fe-based compounds. However, it has the advantage that its results (as far as the amplitude of the gaps are concerned) do not differ significantly from those provided by the much more complicated '3D BTK model' we introduced a few years ago and that accounts for the real shape of the FS [34, 48]. By the way, the use of the 3D BTK model would require at least a qualitative knowledge of the **k**-dependence of the gap, which is not available at present, as discussed above. Moreover, the gaps we have used in the model are isotropic. This is again a simplification, but justified by the shape of the low-temperature spectra (that always show symmetric conductance maxima as expected for a *s*-wave gap) and by the fact that, as shown elsewhere [48], even if there were node lines residing on a nearly-2D Fermi surface (as suggested by nuclear magnetic resonance [12], angle-resolved thermal conductivity [13], nanocalorimetry [14], magnetic penetration depth [11]), they would be hardly detectable in the spectra taken along the *c* axis at finite temperature.

In general, the shift and consequent deformation of the conductance curves prevents their accurate fit up to the critical temperature. As an example, figure 5(a) reports the fits of the conductance curves of figure 3(a). The fit looks good up to 25.8 K, i.e. before the shift of the unnormalized conductance curves begins. At higher temperatures, a different guess normal state must be used for each curve, which necessarily implies a loss of reliability of the fit; moreover, the structures marked by arrows start to interfere with the Andreev-reflection signal. Panel (b) reports the best-fitting values of the gaps as a function of temperature. The uncertainty, evaluated as explained above, is here reported only for a subset of points. The large gap Δ_2 shows a remarkably good BCS-like temperature dependence, while the small gap Δ_1 deviates from the relevant BCS-like curve already at 14.5 K. Panel (c) shows the other fitting parameters. The decrease in Γ_1 and Z_1 observed at high temperature arises from the narrowing of the Andreev features that, in turn, is due to both the spreading resistance and the critical current effects. This decrease is unphysical (Z_1 and Z_2 should be constant, while Γ_1 and Γ_2 should increase with temperature) and simply tells us that the fit is no longer reliable in this region, i.e. at $T \gtrsim 23$ K.

Let us now focus again on the low-temperature gaps and see how they behave as a function of fluence. Figure 6(a) reports the gap amplitudes with the relevant uncertainty (here including the effects of different normalizations) for N.316, N.686 and N.360. Each point here represents the gap amplitude extracted from the fit of a *single* curve at low temperature (4.2 K). The vertical spread of the data for each fluence arises from the fact that all these points come from different spectra of different contacts made in different regions of the films, and also from the fact that the three films actually possess slightly different critical temperatures (see figure 2). Despite this vertical spread, the gaps follow a common, strongly decreasing trend as a function of Φ. The dashed lines in the figure are only guides to the eye but approximately connect the 'average' gap values for each fluence. According to these lines, the large gap Δ_2 goes from about 8 meV in the pristine films to about 6 meV in the most irradiated ones, thus decreasing by about 25%; the small gap goes from about 4 to 2.5 meV thus decreasing by about 37%. Clearly, this is just a very rough estimation of the rates of suppression, subject to a large uncertainty. If one takes the maximum (minimum) gap in the pristine films and the minimum (maximum) gap in the most irradiated ones, one obtains that the rate of suppression is between 11% and 45% for Δ_2 and between 13% and 50% for Δ_1. The important result is however that the decrease of the gap amplitudes upon irradiation shown in figure 6(a) is undoubtedly bigger than that of the critical temperature shown in figure 2. In other words, the gap ratios $2\Delta_{1,2}/k_B T_c$ decrease significantly upon irradiation, as shown in figure 6(b). Even taking into account the vertical spread of data, a horizontal line (corresponding to constant gap ratios) is clearly unable to describe the trend of either $2\Delta_1/k_B T_c$ or $2\Delta_2/k_B T_c$. Note that, because of the difficulty in determining the critical temperature of each contact and following the discussion of figure 3, to calculate the gap ratios we have used the critical temperature of the film measured by transport, i.e.
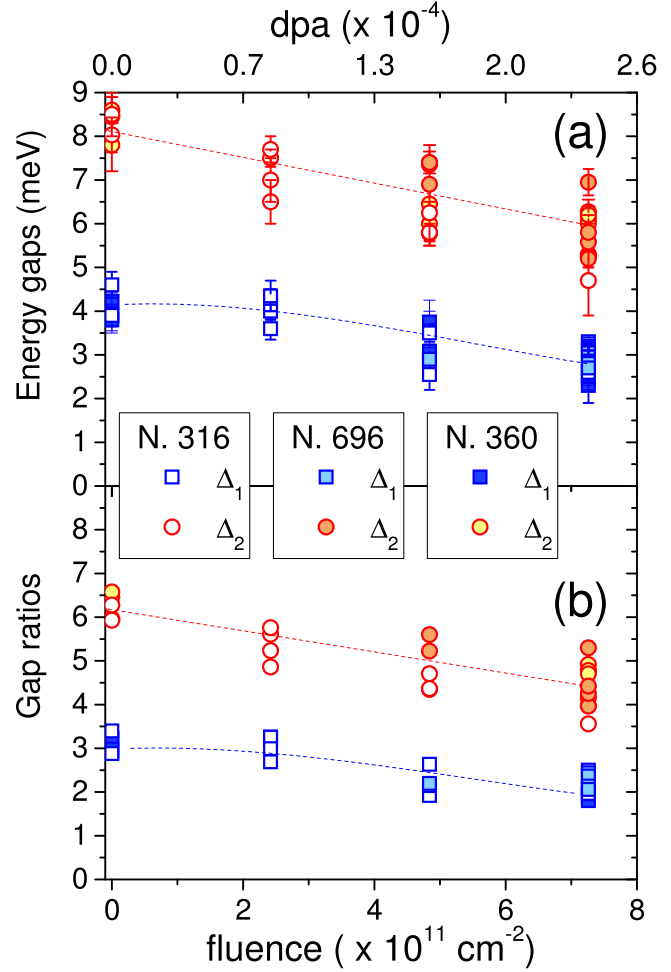

Figure 6. (a) Energy gaps extracted from the fit of the low-temperature conductance curves of the three different films, plotted as a function of the fluence Φ (bottom axis) and of the displacements per atom (dpa, top axis). Note that despite the small difference in critical temperature, the gaps follow the same trend in all the three films. (b) Gap ratios $2\Delta_i/k_B T_c$ (where T_c is that determined from transport, i.e. T_c^{90}) as a function of fluence and dpa. The suppression of the gap ratios is evident.

T_c^{90}. The same result, with only a slight difference in the absolute values, would be obtained by using T_c^{10} instead.

3. Interpretation of the experimental results

The decoupling between the critical temperature and the energy gap amplitudes, which is evident in the modification of the gap ratios, is an interesting and unusual phenomenon. In general, the gap ratio is taken as a rough indication of the strength of the electron–boson coupling. In conventional BCS superconductors, its value is predicted to be $\simeq 3.53$; in MgB_2, which is a two-band phonon-mediated superconductor, the two gap ratios are respectively larger and smaller than this value. When MgB_2 is irradiated with neutrons [37], both the gaps decrease and finally merge into one, whose gap ratio is again approximately BCS. As we showed in [37] the behaviour of the gaps as a function of the critical temperature in irradiated MgB_2 samples cannot be explained by a simple
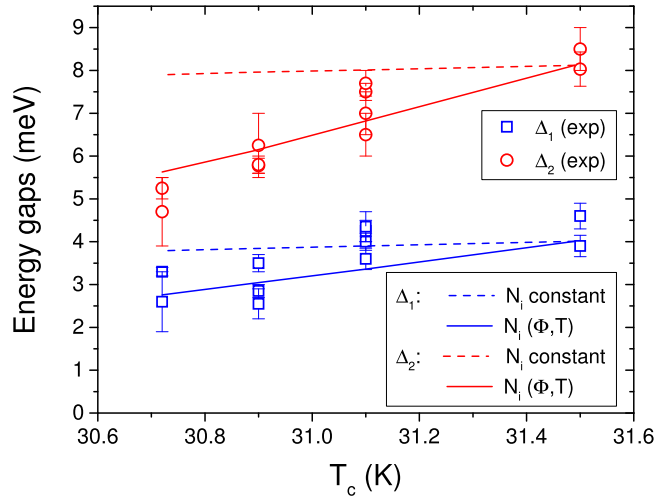
Figure 7. Symbols: the experimental low temperature energy gaps of film N.316 (symbols) as a function of the critical temperature T_c^{90}. Lines: the same quantities calculated by numerical solutions of Eliashberg equations: in the standard case, i.e. with temperature-independent density of states at the Fermi level N_i (dashed lines) and by using temperature-dependent densities of states $N_i(\Phi, T)$ (solid lines).

disorder effect and is instead dominated by a reduction of the σ-band DOS; but in that case the gaps always remain approximately proportional to the critical temperature. What happens here, on the contrary, is that this proportionality is completely broken. A similar trend was evidenced in ultrathin bilayers of conventional superconductors and normal metals (Pb and Ag) [50] where the decrease in T_c as a function of the normal-layer thickness d_N was accompanied by a decrease in the gap ratio well below the BCS value. In that case, a direct evidence was found (by means of tunnel spectroscopy at low temperature) of a finite anomalous subgap density of quasi-particles that increases on increasing d_N. Quoting [50], 'these states cannot contribute to pairing at low temperatures. They can, however, contribute to pairing at high temperatures where the divergence of the coherence length allows them to become untrapped. Thus, the effective DOS available for pairing is higher near T_c than at low temperatures.' In the case of the irradiated thin films of BaFe$_2$(As, P)$_2$ studied here, the existence of subgap states can be easily associated to defects that act as normal regions able to trap charge carriers at low temperature.

To see whether the idea of subgap states being responsible for the decoupling between T_c and energy gaps can be made quantitative, we developed a model based on Eliashberg theory. The model is based on the assumption of a dominant interband coupling mediated by antiferromagnetic spin fluctuations (sf), while the (small) intraband coupling is mediated by phonons (ph), as is the case in most of the Fe-based compounds [51–53].

As already mentioned, ARPES measurements agree about the presence of five Fermi surface sheets: three holelike (α, β, γ) and two electronlike (δ, η). However, taking into account that two holelike bands are nearly degenerate, it is possible to model the compound as a four-band system. The

problem with a four-band model (plus the effect of disorder) is the huge number of free parameters. A substantial simplification can be made by a projection of the four-band model onto an effective two-band model, motivated by the usual observation of two superconducting energy gaps in a variety of experiments, including of course PCARS ones. Since the model is effective, we will neglect the possible anisotropy of the gaps to focus on their amplitudes, i.e. we will assume the two gaps to be isotropic. As expected within the $s\pm$ symmetry [51], Δ_2 has opposite sign compared to Δ_1. Let us warn the reader about the fact that, since the two-band model is an *effective* model, the values of electron–boson coupling do not have an immediate physical interpretation and we can no more divide the phonon and antiferromagnetic spin fluctuation contributions in intraband and interband channels [54]. This means that, for example, the diagonal terms of the coupling-constant matrix, λ_{ii}, contain contributions from both intra and interband terms in the real four-band model.

To calculate the gaps and the critical temperature within the $s\pm$ wave, two-band Eliashberg model [55–57], one has to solve four coupled equations for the gaps $\Delta_i(i\omega_n)$ and the renormalization functions $Z_i(i\omega_n)$, where $i = 1, 2$ is the band index and ω_n are the Matsubara frequencies. The imaginary-axis equations have been reported elsewhere [58–60] and contain several parameters and functions to be determined, whose number can be considerably reduced by using some reasonable approximations.

First of all, the total electron–phonon coupling constant in Fe-based superconductors is small if compared to the electron–boson (spin fluctuation) one [51, 53] so we can neglect the phonon contribution to the superconducting coupling. As a consequence, the coupling constant matrix is completely defined by the electron–boson spectral functions $\alpha^2 F_{i,j}^{\text{sf}}(\Omega)$, that—based on experimental measurements of inelastic neutron scattering [61]—can be chosen to have the form [58–60]

$$\alpha^2 F_{i,j}^{\text{sf}}(\Omega) = C_{ij} \frac{4\Omega\Omega_0}{\left[(\Omega - \Omega_0)^2 + \left(\frac{\Omega_0}{2}\right)^2\right]\left[(\Omega + \Omega_0)^2 + \left(\frac{\Omega_0}{2}\right)^2\right]} \tag{2}$$

that corresponds to the difference between two Lorentzian functions centred at the characteristic spin-fluctuation energy Ω_0 and with HWHM $= \Omega_0/2$. According to the phenomenological law for pnictides, the energy Ω_0 can be fixed to $\Omega_0 = 4.65 k_B T_{c0}$ [49] where $T_{c0} = 31.5$ K is the critical temperature of the pristine film (here, we will refer to one single film, namely N.316). The constants C_{ij} are normalization constants. The fact that they are adjustable means that the electron–boson coupling constants

$$\lambda_{ij}^{\text{sf}} = 2 \int_0^{+\infty} d\Omega \frac{\alpha^2 F_{i,j}^{\text{sf}}(\Omega)}{\Omega} \tag{3}$$

are adjustable parameters of the model. Actually, it can be shown that $\lambda_{ij} = \lambda_{ji} \frac{N_i}{N_j}$ where N_i is the quasiparticle density of states at the Fermi level of the ith equivalent band in the normal state. The values of N_1 and N_2 can be estimated by

starting from the results of ARPES measurements [62], and assuming a free-electron relation between the DOS of each band and the number of charge carriers. The ratio N_1/N_2 turns out to be equal to 0.8.

Thus, only three adjustable elements of the coupling constant matrix remain: λ_{12}, λ_{11} and λ_{22}. In the pristine film, these are the *only* parameters of the model and can be adjusted in order to reproduce the value of the critical temperature $T_{c0} = 31.5$ K and of the low-temperature gaps Δ_1 and Δ_2. We find the following values: $\lambda_{11} = 2.79$, $\lambda_{12} = -0.40$ and $\lambda_{22} = 0.83$. The total coupling constant is $\lambda_{\text{tot}} = \sum_{i,j=1}^{2} N_i \lambda_{ij} / \sum_{i=1}^{2} N_i = 1.35$.

To account for the effect of irradiation, one must include in the model the non-magnetic scattering rates (treated in Born approximation) Γ_{ij}. The terms Γ_{ii} play no role (they cancel out in the equations) and the only parameter remains Γ_{12} because $\Gamma_{21} = \Gamma_{12} N_2 / N_1$. If one keeps the values of the DOS identical to those of the pristine film, i.e. N_1 and N_2, and simply adds disorder (i.e. increases Γ_{12}) it is impossible to reproduce the experimental results in the standard Eliashberg theory. This is clearly shown in figure 7 that reports the experimental gap values of the film N.316 (symbols) as a function of the critical temperature T_c^{90}. The dashed lines represent the values of the gaps calculated by adjusting Γ_{12} so as to obtain the correct critical temperature, and keeping all the other parameters fixed to the 'pristine' values. Clearly, the small decrease in T_c within this model gives rise to a small decrease in the gaps that would be experimentally undetectable, in contrast with the experimental findings.

Based on the aforementioned analysis in ultrathin bilayers, and on the fact that defects induced by irradiation can indeed act as normal regions creating localized subgap normal states, we then allowed the DOS to increase as a function of temperature, because of the divergence in the coherence length that makes these states available for pairing at high temperature [50].

The simplest assumption we can make is that the reduction in the DOS at low temperature upon irradiation, i.e. $N_i(\Phi, T=0) - N_i$ is *linearly* dependent on the disorder, i.e. on Γ_{12} (which is the non-magnetic scattering rate). With this assumption, the temperature dependence of the density of states that allows reproducing the experimental data turns out to be quadratic

$$N_i(\Phi, T) = N_i[1 - a(T_c(\Phi) - T)^2]$$
$$= N_i[1 - b/\xi^4(T)], \quad (4)$$

where $\xi(T)$ is the superconducting coherence length. Equation (4) means that the functional form of the dependence of $N_i(\Phi, T)$ on T is universal, but the coefficient a linearly depends on disorder, i.e. $a = k\Gamma_{12}$ (with k adjustable parameter). We have explicitly indicated that also T_c depends on Φ. In this way also the coupling constants, which are proportional to the normal density of states at the Fermi level, depend on temperature and disorder. As a matter of fact, $\lambda_{ii}(\Phi, T) = \lambda_{ii} N_i(\Phi, T)/N_i$ so that

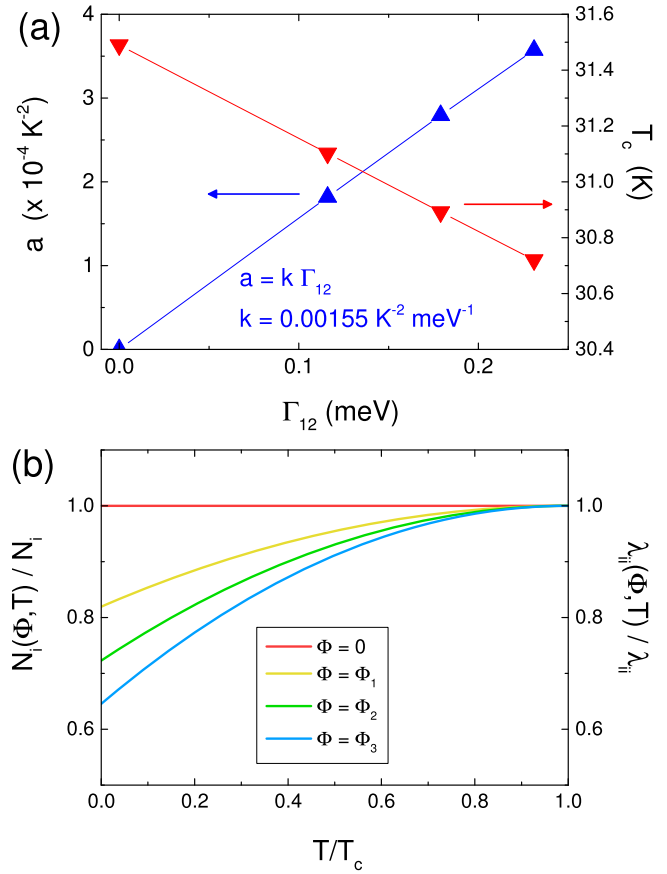$$\frac{\lambda_{ii}(\Phi, T)}{\lambda_{ii}} = \frac{N_i(\Phi, T)}{N_i} = 1 - a(T_c(\Phi) - T)^2 \quad (5)$$

Figure 8. (a) The critical temperature T_c (right-hand vertical axis, down triangles) and the parameter a (left-hand vertical axis, up triangles) as a function of Γ_{12}. (b) Temperature dependence of the normalized densities of states $N_i(\Phi, T)/N_i$ and of the normalized intraband coupling constants $\lambda_{ii}(\Phi, T)/\lambda_{ii}$ that allow reproducing the experimental values of the critical temperature and of the energy gaps.

while the value of λ_{12} does not change upon irradiation. Now, we are thus left with two free parameters, Γ_{12} and k, that can be tuned in order to reproduce the experimental T_c and the low-temperature gap values. Γ_{12} is completely determined by the critical temperatures of the irradiated films, because at the onset of the superconducting transition the density of states is always equal to the unperturbed value, i.e. N_i, irrespective of the disorder. The relationship between the resulting values of Γ_{12} and T_c is linear and is reported in figure 8(a) (bottom and right axes, down triangles). The low-temperature gap values depend not only on Γ_{12} but also on the low-temperature density of states, and thus on k because of equation (4). The value of k that allows reproducing the low-temperature gap amplitudes for all the irradiation levels is $k = 0.00155$ K^{-2} meV^{-1}; this is the slope of the a versus Γ_{12} curve reported in figure 8(a) (bottom and left axes, up triangles). The temperature dependence of the coupling constants and of the DOSs normalized to their unperturbed values (that has the form of equation (5)) is shown in figure 8(b).

The gap amplitudes calculated by solving the Eliashberg equations using the values of k and Γ_{12} shown in figure 8(a) are reported in figure 7 as a function of the critical temperature of the films (solid lines). The figure clearly shows that it

is possible to approximately reproduce the experimental trend of the gaps with a minimal number of parameters. Therefore, the observed decoupling between the energy gaps and the critical temperature can be explained by a temperature dependence of the density of states at the Fermi level that is, in turn, due to the presence of defects. Once the values of the coupling constants in the pristine film are fixed so as to give the correct T_c and gap amplitudes, the disorder-dependence of the same quantities is completely reproduced by assuming a simple linear relation between the irradiation-induced reduction in the density of states at low temperature and the non-magnetic scattering rate Γ_{12}.

4. Conclusions

We have studied the effects of irradiation with 250 MeV Au ions on the superconducting properties (critical temperature and energy gaps) of three different thin epitaxial films of $BaFe_2(As_{1-x}P_x)_2$ close to optimal doping. The critical temperature, determined by means of transport measurements, decreases only slightly (of about 3%) upon irradiation up to a fluence $\Phi_3 = 7.3 \times 10^{11}$ cm^{-2} that corresponds to about 2.5×10^{-4} dpa in the thin film. The energy gaps were measured by point-contact Andreev-reflection spectroscopy by using the so called 'soft' technique. The point-contact spectra often show non-ideal features at high voltage and high temperature, due to the current-induced breakdown of superconductivity and to the onset of a finite spreading resistance close to the resistive transition of the film. However, we could obtain various contacts in the spectroscopic regime (at least at low temperature) whose spectra display structures associated to two different and well-separated energy gaps Δ_1 and Δ_2. No clear sign of node lines was visible in the spectra, taken with the current mainly injected along the c axis. The fit of the spectra with a two-band, 2D BTK model using two isotropic gaps gave us the amplitudes of the two gaps that, in the pristine films, are $\Delta_1 \simeq 4$ meV and $\Delta_2 \simeq 8.5$ meV. Upon irradiation, both the gaps strongly decrease in an almost linear way as a function of the fluence, so that at $\Phi = \Phi_3$ they are reduced by about 37% and 25%, respectively.

The much larger rate of suppression of the gaps if compared to that of the critical temperature makes the gap ratios decrease as a function of the fluence, indicating an irradiation-induced decoupling between the gaps and T_c. This behaviour cannot be explained by simply invoking the effect of disorder (i.e. an increase in the scattering rates). Instead, it can be rationalized as being due to defected (normal) regions in the film that create low-energy quasiparticle states. At low temperature these states are localized (trapped by defects) and unavailable for pairing, but at high temperature they become untrapped because of the divergence of ξ. Hence, the density of states available for pairing increases with temperature. Within an effective two-band model in the Eliashberg theory, this temperature dependence turns out to be quadratic, if a linear relationship is assumed between the suppression in the

low-temperature density of states and the parameter Γ_{12} that is a measure of the disorder.

ORCID iDs

Renato S Gonnelli ⬤ https://orcid.org/0000-0001-7108-8458

References

[1] Nakajima Y, Taen T, Tsuchiya Y, Tamegai T, Kitamura H and Murakami T 2010 *Phys. Rev.* B **82** 220504(R)
[2] Mizukami Y *et al* 2014 *Nat. Commun.* **5** 5657
[3] Cho K, Konczykowski M, Murphy J, Kim H, Tanatar M A, Straszheim W E, Shen B, Wen H H and Prozorov R 2014 *Phys. Rev.* B **90** 104514
[4] Ghigo G, Ummarino G A, Gozzelino L, Gerbaldo R, Laviano F, Torsello D and Tamegai T 2017 *Sci. Rep.* **7** 13029
[5] Wang Y, Kreisel A, Hirschfeld P J and Mishra V 2013 *Phys. Rev.* B **87** 094504
[6] Schilling M B *et al* 2016 *Phys. Rev.* B **93** 174515
[7] Efremov D V, Korshunov M M, Dolgov O V, Golubov A A and Hirschfeld P J 2011 *Phys. Rev.* B **84** 180512(R)
[8] Daghero D, Tortello M, Gozzelino L, Gonnelli R S, Hatano T, Kawaguchi T and Ikuta H 2017 *Appl. Surf. Sci.* **395** 9–15
[9] Massee F, Sprau P O, Wang Y L, Séamus Davis J C, Ghigo G, Gu G and Kwok W K 2015 *Sci. Adv.* **1** e1500033
[10] Nakajima Y, Tsuchiya Y, Taen T, Tamegai T, Okayasu S and Sasase M 2009 *Phys. Rev.* B **80** 012510
[11] Hashimoto K *et al* 2010 *Phys. Rev.* B **81** 220501
[12] Nakai Y, Iye T, Kitagawa S, Ishida K, Kasahara S, Shibauchi T, Matsuda Y and Terashima T 2010 *Phys. Rev.* B **81** 020503(R)
[13] Yamashita M *et al* 2011 *Phys. Rev.* B **84** 060507
[14] Campanini D, Diao Z, Fang L, Kwok W K, Welp U and Rydh A 2015 *Phys. Rev.* B **91** 245142
[15] Shimojima T *et al* 2011 *Science* **332** 564–7
[16] Zhang Y, Ye Z R, Ge Q Q, Chen F, Jiang J, Xu M, Xie B P and Feng D L 2012 *Nat. Phys.* **8** 371–5
[17] Shimojima T *et al* 2012 *Solid State Commun.* **152** 695–700
[18] Yoshida T *et al* 2014 *Sci. Rep.* **4** 7292
[19] Kawaguchi T, Sakagami A, Mori Y, Tabuchi M, Ujihara T, Takeda Y and Ikuta H 2014 *Supercond. Sci. Technol.* **27** 065005
[20] Sakagami A, Kawaguchi T, Tabuchi M, Ujihara T, Takeda Y and Ikuta H 2013 *Physica* C **494** 181
[21] Kurth F *et al* 2015 *Appl. Phys. Lett.* **106** 072602
[22] Kasahara S *et al* 2010 *Phys. Rev.* B **81** 184519
[23] Koon D and Knickerbocker C J 1996 *Rev. Sci. Instrum.* **67** 4282

[24] Koon D and Chan W K 1998 *Rev. Sci. Instrum.* **69** 4218
[25] Gerbaldo R, Ghigo G, Gozzelino L, Laviano F, Amato A, Rovelli A and Cherubini R 2013 *AIP Conf. Proc.* **1530** 95–102
[26] Ziegler J http://srim.org/
[27] Ziegler J F, Ziegler M D and Biersack J P 2010 *Nucl. Instrum. Methods Phys. Res.* B **268** 1818
[28] Stoller R E, Toloczko M B, Was G S, Certain A G, Dwaraknath S and Garner F A 2013 *Nucl. Instrum. Methods Phys. Res.* B **310** 75–80
[29] Norgett M J, Robinson M T and Torrens I M 1975 *Nucl. Eng. Des.* **33** 50
[30] Pecchio P, Daghero D, Ummarino G A, Gonnelli R S, Kurth F, Holzapfel B and Iida K 2013 *Phys. Rev.* B **88** 174506
[31] Daghero D, Pecchio P, Ummarino G, Nabeshima F, Imai Y, Maeda A, Tsukada I, Komiya S and Gonnelli R S 2014 *Supercond. Sci. Technol.* **27** 124014
[32] Sharvin Y V 1965 *Zh. Eksp. Teor. Fiz.* **48** 984
Sharvin Y V 1965 *Sov. Phys. JETP* **21** 655
[33] Wexler G 1966 *Proc. Phys. Soc. London* **89** 927
[34] Daghero D and Gonnelli R 2010 *Supercond. Sci. Technol.* **23** 043001
[35] Naidyuk Y G and Yanson I K 2004 *Point-Contact Spectroscopy* (*Springer Series in Solid-State Sciences* vol 145) (Berlin: Springer)
[36] Deutscher G 2005 *Rev. Mod. Phys.* **77** 109–35
[37] Daghero D, Calzolari A, Ummarino G A, Tortello M, Gonnelli R S, Stepanov V A, Tarantini C, Manfrinetti P and Lehmann E 2006 *Phys. Rev.* B **74** 174519
[38] Sheet G, Mukhopadhyay S and Raychaudhuri P 2004 *Phys. Rev.* B **69** 134507
[39] Chen T Y, Huang S X and Chien C L 2010 *Phys. Rev.* B **81** 214444
[40] Döring S, Schmidt S, Gottwals S, Schmidl S, Tympel V, Mönch I, Kurth F, Iida K, Holzapfel B and Seidel P 2014 *J. Phys.: Conf. Ser.* **507** 012008
[41] Kashiwaya S, Tanaka Y, Koyanagi M and Kajimura K 1996 *Phys. Rev.* B **53** 2667
[42] Kashiwaya S and Tanaka Y 2000 *Rep. Prog. Phys.* **63** 1641–724
[43] Plecenik A, Grajcar M, Beňačka V, Seidel P and Pfuch A 1994 *Phys. Rev.* B **49** 10016

[44] Pogrebna A, Mertelj T, Ye Z R, Feng D L and Mihailovic D 2015 *Phys. Rev.* B **92** 144503
[45] Daghero D, Delaude D, Calzolari A, Tortello M, Ummarino G A, Gonnelli R S, Stepanov V A, Zhigadlo N D, Katrych S and Karpinski J 2008 *J. Phys.: Condens. Matter* **20** 085225
[46] Daghero D, Tortello M, Gonnelli R S, Stepanov V A, Zhigadlo N D and Karpinski J 2009 *Phys. Rev.* B **80** 060502(R)
[47] Tortello M, Daghero D, Ummarino G A, Stepanov V A, Jiang J, Weiss J D, Hellstrom E E and Gonnelli R S 2010 *Phys. Rev. Lett.* **105** 237002
[48] Daghero D, Tortello M, Ummarino G and Gonnelli R S 2011 *Rep. Prog. Phys.* **74** 124509
[49] Paglione J and Greene R L 2010 *Nat. Phys.* **6** 645–58
[50] Long Z, Stewart M D and Valles J M 2006 *Phys. Rev.* B **73** 140507
[51] Mazin I I, Singh D J, Johannes M D and Du M H 2008 *Phys. Rev. Lett.* **101** 057003
[52] Mazin I I and Schmalian J 2009 *Physica* C **469** 614
[53] Boeri L, Calandra M, Mazin I I, Dolgov O V and Mauri F 2010 *Phys. Rev.* B **82** 020506-1–4
[54] Charnukha A, Dolgov O V, Golubov A A, Matiks Y, Sun D L, Lin C T, Keimer B and Boris A V 2011 *Phys. Rev.* B **84** 174511
[55] Eliashberg G M 1963 *Sov. Phys. JETP* **11** 696
[56] Chubukov A V, Pines D and Schmalian J 2008 A spin fluctuation model for d-wave superconductivity *Superconductivity* (Berlin: Springer) pp 1349–413
[57] Manske D, Eremin I and Bennemann K H 2008 Electronic theory for superconductivity in high-T_c cuprates and Sr_2RuO_4 *Superconductivity* (Berlin: Springer) pp 1415–515
[58] Ummarino G A, Tortello M, Daghero D and Gonnelli R S 2009 *Phys. Rev.* B **80** 172503-1–4
[59] Ummarino G A, Daghero D, Tortello M and Gonnelli R S 2011 *J. Supercond. Novel Magn.* **24** 247–53
[60] Ummarino G A 2011 *Phys. Rev.* B **83** 092508-1–4
[61] Inosov D S *et al* 2010 *Nat. Phys.* **6** 178–81
[62] Ye Z R, Zhang Y, Chen F, Xu M, Ge Q Q, Jiang J, Xie B P and Feng D L 2012 *Phys. Rev.* B **86** 035136